Geomorphology 329 (2019) 17–31

Contents lists available at ScienceDirect

Geomorphology

journal homepage: www.elsevier.com/locate/geomorph

Historical evolution and controls on mega-blowouts in northeastern Qinghai-Tibetan Plateau, China

Wanyin Luo [a,b,*], Zhongyuan Wang [a,c], Mei Shao [a], Junfeng Lu [a], Guangqiang Qian [a], Zhibao Dong [a,d], Patrick A. Hesp [e], Mark D. Bateman [b]

[a] Key Laboratory of Desert and Desertification, Northwest Institute of Eco-Environment and Resources, Chinese Academy of Sciences, Lanzhou 730000, China
[b] Geography Department, Sheffield University, Winter Street, Sheffield S10 2TN, UK
[c] State Key Laboratory of Earth Surface Processes and Resource Ecology, Beijing Normal University, Beijing 100875, China
[d] School of Geography and Tourism, Shaanxi Normal University, Xi'an, China
[e] Beach and Dune Systems (BeaDS) Laboratory, College of Science and Engineering, Flinders University, Sturt Road, South Australia 5042, Australia

ARTICLE INFO

Article history:
Received 24 July 2018
Received in revised form 27 December 2018
Accepted 28 December 2018
Available online 4 January 2019

Keywords:
Mega-blowouts
Qinghai-Tibet Plateau
Morphodynamics
Control factors

ABSTRACT

Mega-blowouts are very large-scale deflationary landforms, formed by wind erosion. They are abundant in the Gonghe basin, northeast margin of the Qinghai-Tibet Plateau (QTP) and little is known about the evolution, dynamics or controls on the mega-blowout development. Here we report on mega-blowouts' morphodynamic expansion rates based on 4 years of monitoring. Also presented is a remotely sensed longer-term (48 years) morphologic change record which is used to understand the initiation, growth and evolution of mega-blowouts in alpine grasslands. Links between the morphodynamics and blowout-controlling factors are analysed. The expansion rates of the monitored blowouts vary according to blowout area, with different parts of the blowouts expanding at different rates. Generally longitudinal (downwind) mega-blowout expansion is greatest, with upwind headwall expansion via collapse being particularly significant. The growth of depositional lobes downwind of mega-blowouts tends to be faster than growth of the deflation basins. Merging of adjacent blowouts is one of the key mechanisms for mega-blowout development and extension. Sediment characteristics, wind erosion, water erosion, and freeze-thaw processes also all play a part in mega-blowout initiation and expansion. However, the relative roles that these factors play may differ according to a blowout's evolutionary stage. Due to an almost unlimited depth of sand, very low water table, and short grass vegetation cover, evolution into parabolic dunes is limited. A large proportion of sand patches and small blowouts around the mega-blowouts are still developing in the Gonghe basin proving that land degradation is still ongoing. Future work will focus on the feedback mechanisms between the blowout morphodynamics, climate change and anthropogenic impacts.

© 2019 Elsevier B.V. All rights reserved.

1. Introduction

A blowout is a rectangular to concave trough, bowl or saucer-shaped hollow formed by wind erosion of the original sandy sediments (Carter et al., 1990; Hesp, 2002). Generally, it is initiated in pre-existing sand, silt, and/or clay deposits by surface disturbance and/or depletion of vegetation cover induced by climate change, human and animal activities, or other factors (e.g. coastal erosion) (Carter et al., 1990; Hesp, 2002; Hesp and Walker, 2012, 2013; Smyth et al., 2012). Even though initiated by erosion, blowouts also possess an associated depositional lobe and thus, they are composed of both erosional and depositional features (Gares and Nordstrom, 1995). Blowout formation often signals the reactivation of previously fixed dunes and has been considered as the direct response of landscape to climate change and human activities in beach and inland, dry, arid-regions (Barchyn and Hugenholtz, 2013). Blowouts are found throughout the equatorial to high-latitude regions, especially in arid and semi-arid sandy grasslands or coastal zones (Hugenholtz and Wolfe, 2006; Ruz and Hesp, 2014). Due to the differences in sedimentary and geomorphological characteristics of the substrata, blowout shapes are also variable. However, they can basically be divided into four kinds of forms: sand patch, shallow saucer, bowl, and trough, sometimes representing different development stages of blowouts (Hesp, 2002; Hesp et al., 2016). Reported depths of blowouts are mostly <10–15 m (Cooper, 1958; Jungerius et al., 1981; Pluis, 1992; Hugenholtz and Wolfe, 2006, 2009; Hesp et al., 2016), but recent field surveys have found large numbers of blowouts in the northeastern Qinghai-Tibet Plateau (QTP) with up to 40 m deep, here termed mega-blowouts (Luo et al., 2018). Deflation landscapes of such large size/depth are rare in the world and systematic studies are needed to

* Corresponding author at: Northwest Institute of Eco-Environment and Resources, Chinese Academy of Sciences, No. 320, West Donggang Road, Lanzhou, Gansu Province 730000, China.
E-mail address: wyluo@lzb.ac.cn (W. Luo).

https://doi.org/10.1016/j.geomorph.2018.12.033
0169-555X/© 2019 Elsevier B.V. All rights reserved.

understand how and why such landscapes have formed and continue to form in the QTP.

The Gonghe basin, our study site in the Qinghai-Tibet Plateau is located in the intersection of the westerlies wind belt and Asia and India monsoon region (Fig. 1). It is an important part of the desert-loess boundary belt and a particularly vulnerable zone of the landscape (Dong et al., 2017; Qiang et al., 2016). The unique geographical location and fragile ecosystem make it extremely sensitive to global change, and a key area to study for climate and environmental changes of the Qinghai-Tibet Plateau. Previous research on palaeoclimate, palaeoenvironmental

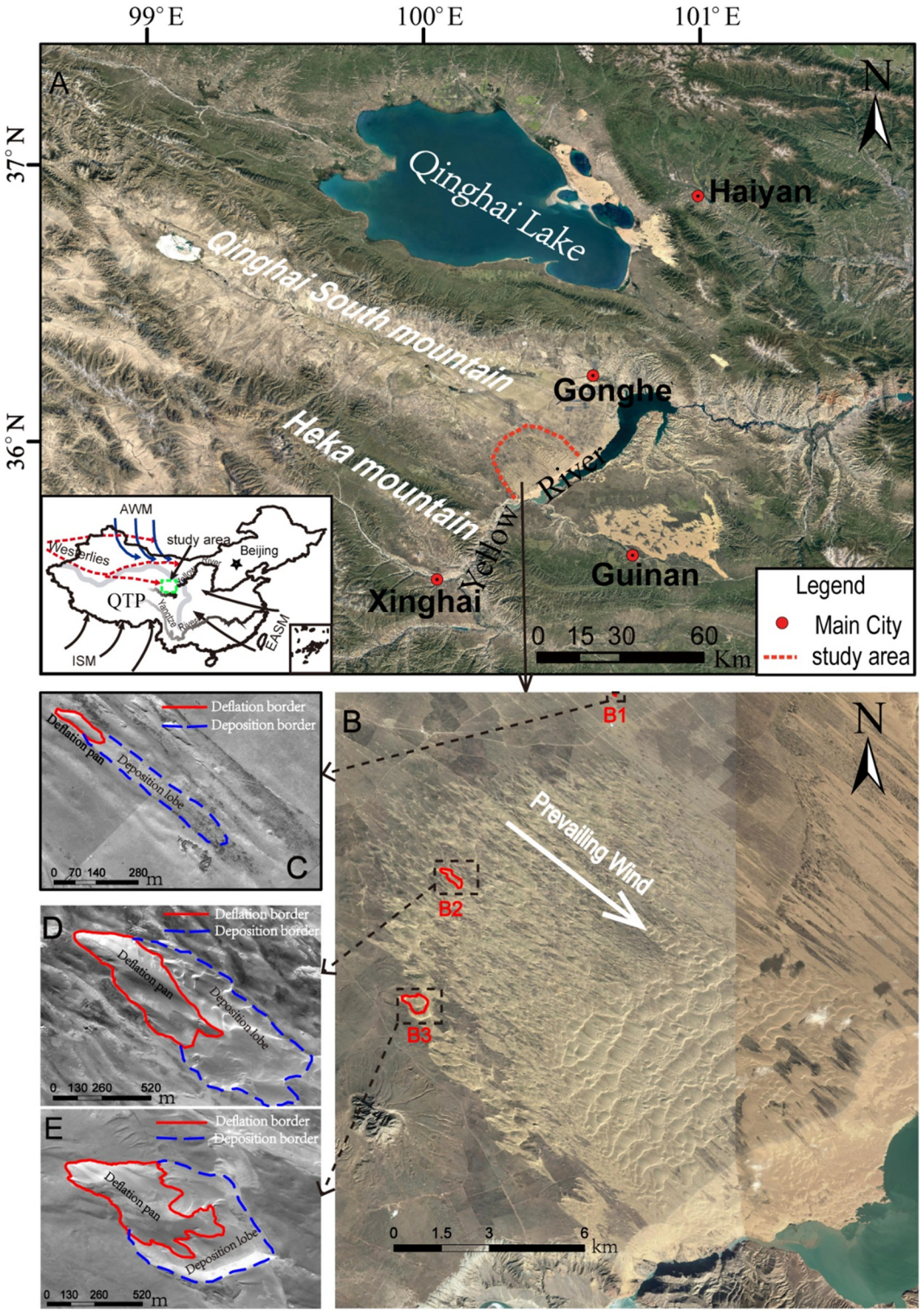

Fig. 1. Topographic map of China and typical mega-blowouts in Qinghai-Tibet Plateau (QTP). (A) landscape map of the study area and its major atmospheric systems, AWM = Asian winter monsoon, ISM = Indian summer monsoon, EASM = East Asian summer monsoon; (B) satellite image of the research site, the red polygons represent the three monitored mega-blowouts. The mega-blowouts are mainly distributed on the upwind edge of the activated dunes. (C–E) high-resolution image of monitored blowouts (Worldview II, 2008), showing both the size and the border of the deflation basin or plain and the depositional lobe.

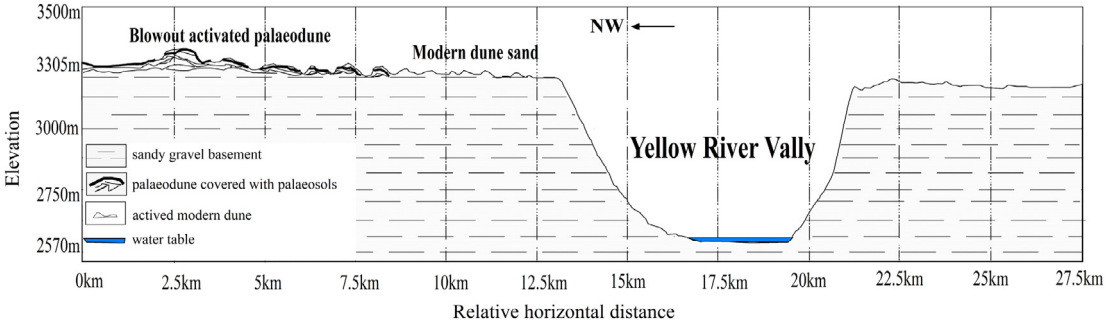

Fig. 2. Landform profile of Santala plateau, Gonghe basin.

change and evolution of the wind regime in the Gonghe basin (Xu et al., 1984; Dong et al., 1993) found four cold phases since the last glacial maximum. More recently, Qiang et al. (2016) and Liu et al. (2013) using magnetic susceptibility, carbon content, grain size, and geochemical parameters combined with OSL dating found aeolian activity occurred episodically during the Holocene period, and a cold and dry stage started 0.7 ka from present. Before the work of Luo et al. (2018), mega-blowouts' formation and their evolutionary processes in this region had not been described or studied in detail (Dong et al., 1993).

With the development of aeolian sand dune research, more attention has been paid to studies on blowout flow dynamics (Hesp and Hyde, 1996; Fraser et al., 1998; Hesp et al., 2017), wind regimes (Jungerius et al., 1991; Hesp et al., 2016), sedimentary structures (Villanueva et al., 2011) and spatial-temporal evolution of coastal blowouts (Jungerius and Meulen, 1989; Carter et al., 1990; Smyth et al., 2012; Hesp and Pringle, 2001). Coastal blowout initiation was proposed by Hesp (2002) and Hesp et al. (2016) to be water erosion, topographic wind acceleration, climate change, disruptions to vegetation succession, wave and wind erosion, and human/animal activities. However, it has been suggested by some that blowout growth is not infinite and there is a critical form to which they evolve (Hugenholtz and Wolfe, 2006). Hugenholtz and Wolfe (2006) confirmed this idea through long-term field monitoring of blowouts which revealed that the erosion was weak at the bottom of the erosion pan if the critical morphology is reached.

Blowout development can lead to the reactivation of palaeodunes (Luo et al., 2018) and the release of dust into the atmosphere with large-scale environmental effects (Dong et al., 1993). In addition, blowout development has been shown to have some sensitivity to climate change and human activities (Hugenholtz and Wolfe, 2006; Zhang et al., 2006; Hugenholtz and Wolfe, 2009; Hesp et al., 2016). However, due to a lack of systematic research at a landscape level or for inland, mega-blowouts in alpine cold regions such as in the QTP, the connections between mega-blowout development and evolution and climatic changes is still unclear. The IPCC 2013 report showed that the Earth's arid or semi-arid areas will become drier in the next 100 years, which may indicate that dune reactivation, blowout formation and dust/sandstorm activities will be higher and more intense in the future. Our ability

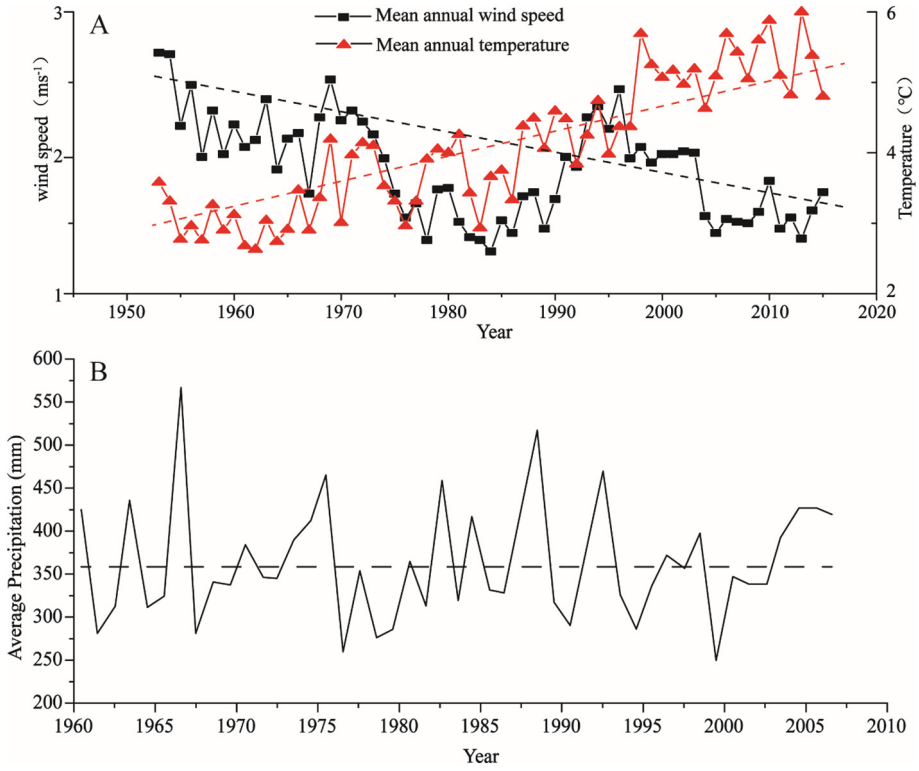

Fig. 3. Historic meteorological conditions in the research area. A. 63-years wind speed and temperature variation with trends line, B. 45-years precipitation variation with trends line. Data provided by the Meteorological Network, China Meteorological Administration (Hainan meteorological station, E100°37′, N36°16′, http://data.cma.cn/).

to predict sand dune mobility caused by blowout initiation for future climate change is still limited due to the lack of detailed case studies (Barchyn and Hugenholtz, 2013). This paper aims to provide a detailed case study from trough mega-blowouts which are typical blowout types in the Gonghe Basin, northeastern QTP. Real-time kinematic GPS monitoring over 4 years is utilized to understand morphodynamic expansion rates of blowouts. A GIS-based 50-year historical record is presented and used to better understand long-term morphologic change of the mega-blowouts and their controlling factors. The findings are used to enhance our understanding and interpretation of the geomorphic response to future global warming in cold alpine, arid regions.

2. Regional setting and methods

2.1. Regional setting

The study was conducted on the Santala Terrace of the Yellow River in the Gonghe basin at the northeastern edge of the Qinghai-Tibet Plateau (QTP), (Fig. 1A). It is situated south of Qinghai Lake, separated from it by the Qinghai Nan Mountains. The Gonghe Basin lies at the convergence of the Asian summer monsoons, the winter monsoons, and the westerlies, which makes it an important component of the transition zone (Fig. 1A). The basin has been tectonically uplifted to a height of ~500 m relative to the Yellow River since the Late Pleistocene, which has given the basin a complex topography. It also has diverse vegetation types and has an average altitude around 3000 m (Xu et al., 1982). On the eastern residual plains left by incision of Yellow River, the previously deposited fluvial-lacustrine sediments provide abundant fine-grained material for deflation and redeposition (Xu et al., 1982).

There are mainly two types of dunes in the basin, including fixed palaeodunes and active dunes which were formed on these planation surface, 500 m above the Yellow River (Fig. 2), during the two dry periods of the Holocene 6000 years ago and 3000 years ago. So, the deep deposit of sand in this region is dry and the highest seasonal water table is very low (Xu et al., 1984). Thus, there is on seasonal water table to limit the deflation depth, which combined with the continued drought and windy climate promoted the palaeodune reactivation, and hence, the initiation of the mega-blowouts.

The region is dominated in some areas by multiple blowouts, and several are massive in both depth and length. In fact, they are the largest blowouts recorded to date - they are up to 40 m deep and 1 to 1.5 km long and, thus, are termed mega-blowouts by Luo et al. (2018). They are not parabolic dunes as they do not display trailing ridges which is a defining landform unit of parabolic dunes (Nield and Baas, 2008; Hesp and Walker, 2013; Yan and Baas, 2015). According to our field observations and previous dating results (Luo et al., 2018), the blowouts in the QTP formed at three different times. The oldest mega-blowouts which was formed ~500 years ago, corresponding to the dry periods of the Little Ice Age. The younger, small blowouts were initiated in the last few decades to one hundred years ago, and some newly emerged blowouts and sand patches have developed in recent years (Luo et al., 2018). All these different aged groups of blowouts have different morphologies and hence, have possibly or likely different trigger mechanisms. So, in the following we only report the mega-blowouts' evolution and their controlling factors utilizing high resolution in-situ field data supported by remote sensing.

The monitored mega-blowouts formed in the palaeodunes on the Santala terrace in the west bank of Longyangxia Reservoir (Figs. 1B, 2), where the palaeo-sandy deposition is abundant, and the wind-driven degradation of lands takes place frequently. Aeolian activity in this area is prevalent, resulting in extensive dune fields in the basin. Grassland constitutes the main body of the vegetation in Gonghe basin (Dong et al., 1993). The mean annual temperature has continually increased during the past 63 years as recorded by the nearest local meteorological station (Hainan meteorological station, E100°37′, N36°16′). The perennial mean air temperature is 4.0 °C, the highest and lowest monthly mean temperature is 22.1 °C and − 18 °C in July and January, respectively, with the extremely low temperature is −28.9 °C on 13th January in 1961 (Zhang, 1991). The annual mean precipitation varies between 250 and 450 mm, with the annual mean precipitation being around 350 mm during the past 45 years (Fig. 3). The rainfall is mainly concentrated in May and September, accounting for >80% of the annual rainfall. In the dry season from October to April there is little precipitation due to the presence of the Mongolian high pressure and downdraft system (Dong et al., 1993).

The automatic weather station which we constructed near B1 recorded an entire year wind regime from August 2015 to July 2016 (Fig. 4). The mean annual wind speed of the study area was 3.4 m/s, and the maximum wind speed was 30.5 m/s. The annual drift potential (DP) and resultant drift potential (RDP) at the research site is 446 VU (vector units) and 316 VU with a narrow and moderate directional variability (RDP/DP = 0.71) calculated using Fryberger's and Deans' (1979) equation. Furthermore, the data show that the sand drift potential in spring and autumn are much larger than summer and autumn.

2.2. Morphological monitoring methods

2.2.1. Topographic morphological monitoring

In this study, three different sized mega-blowouts were selected as representative of relatively small, medium and large mega-blowouts based on a satellite image overview of all the blowouts in the region. The recent annual expansion rate of the three blowouts was determined using high precision real-time kinematic positioning technology (RTK-GPS, Topcon GR-3) with a horizontal accuracy around 10–20 mm, and vertical accuracy around 20–30 mm. For blowout B1, monitoring data were obtained for five periods (July 2014, July 2015, July 2016, January 2017 and January 2018). For the other two sites (B2 and B3) four periods of monitoring data were obtained (January 2015, March 2016, January 2017 and January 2018).

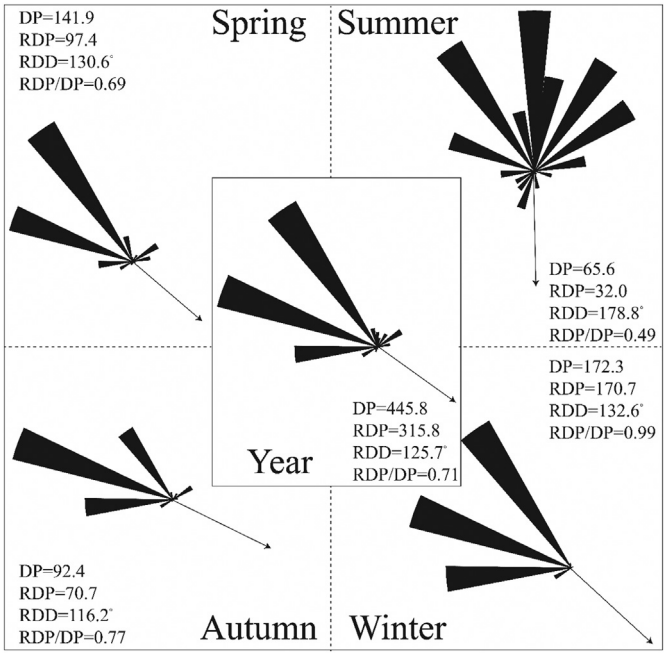

Fig. 4. The wind tower reported seasonal and annual sediment transport potential in the study area from August 2015 to July 2016. The wind condition was divided by the standard delimitation proposed by Fryberger and Dean' equation (1979): $DP = V\ (V - V_{*t})\ t^2$. Where DP is the sand drift potential expressed in vector units (VU), RDP is the resultant drift potential and RDP/DP is the directional variability of wind V is the mean wind velocity at 10 m height for the time period t, the unit is ms^{-1}; V_{*t} is the friction thresh hold wind velocity of sand at 10 m height, 6 ms^{-1} is used in this research. t is sand transport wind time expressed as the percentage in a wind summary (%).

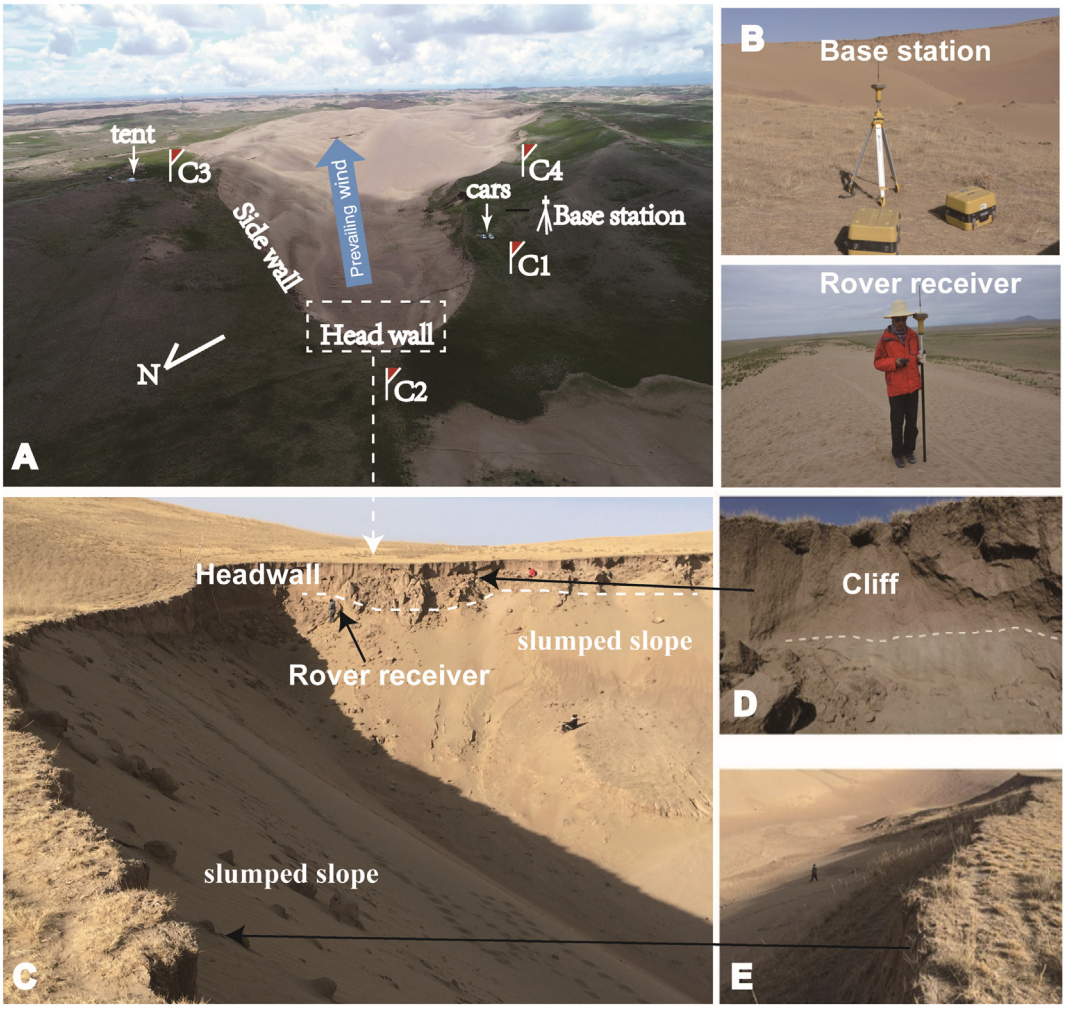

Fig. 5. Geomorphic features of the monitored mega-blowout and the equipment and ground control system. A. top view of blowout B3 as well as the measuring control system, C1, C2, C3 and C4 are the control pint. Note the tent and the cars for the scale comparison; B. RTK-GPS base station and rover receiver; C–E. typical features of different part of mega-blowout. Notice the head wall depth and the cliff height and massive falling block, and humans (arrowed) for scale.

For topographical measurement, a base station was set up adjacent to the blowouts to act as a GPS data receiver and signal transmitting antenna. A rover receiver station with hand-held controllers was used to calculate precise relative position between the base station and the measured point (Fig. 5B). In order to precisely determine blowout margins, high resolution measurements were taken every 5 to 10 cm along the edge of the sidewalls and headwalls especially in the severely eroding and collapsing portions (upwind head wall and side wall). Coarser measurements (5 to 10 m) were conducted within the deflation basin and the downwind depositional lobe. Between 2500 and 3500 data points were sampled during each field measurement. At the same time, four control points (Fig. 5A) around the mega-blowouts were selected to make the local ground co-ordinate transformation and calculate control to ensure the reliability of each measurement comparison. After each measurement was completed, all the measured point data was transformed into grid data, through Kriging interpolation using geosystem software (Surfer 13.6) to draw the 3D surface map (DSM). The edge of the blowout was then extracted manually according to

Table 1
Data sources for remote sensing and the uncertainties evaluated using the RTK-GPS measured ground control points in field for the aerial photos and satellite images.

Aerial photos												
Year	Scale	Distance ratio	Ground control points error (m)									
			1		2		3		4		Mean	
1967	1:6000	0.84	±1.2		±6.9		±7.2		±0.9		±5.0	
Satellite images												
Year	Resource	Pixel resolution	Ground control points error (m)									
			1	2	3	4	5	6	7	8	9	10	11	Mean
2008	DigitalGlobe	0.5 m	±0.2	±1.5	±3.5	±1.5	±1.0	±1.2	±1.5	±1.1	±2.2	±2.8	±4.7	±1.9
2012	DigitalGlobe	0.5 m	±1.2	±1.5	±2.7	±2.1	±1.4	±3.2	±2.5	±1.1	±2.9	±2.5	±3.2	±2.0
2015	DigitalGlobe	0.5 m	±0.5	±1.0	±1.5	±1.0	±1.5	±1.8	±1.5	±1.4	±0.5	±1.0	±5.0	±1.7

Table 2
48-years morphological parameters of the three target blowouts.

Blowouts number	1967			2008			2015		
	Length (m)	Width (m)	Area (m^2)	Length (m)	Width (m)	Area (m^2)	Length (m)	Width (m)	Area (m^2)
B1	–	–	200	158	40	4762	158	46	5178
B2	516	169	131,678	731	186	148,868	743	188	155,009
B3	673	168	149,700	829	225	193,809	827	224	193,186

the point data and post layer margin. Furthermore, the annual and total expansion rates were calculated through comparison between the edge expansion in the different parts of the mega-blowouts across different monitoring seasons or years (Fig. 5D–E).

2.2.2. Remote monitoring

High-resolution satellite images and historical aerial photographs for different periods were used to compare the blowouts two-dimensional long-term morphological expansion. The data source used for this part of the interpretation work was the high-resolution remote sensing images acquired in January 2008, and January 2015 as shown in Fig. 9, which have a spatial resolution of 0.5 m. Firstly, the coordinate transformation was corrected for the two images, so that they had a unified geographic coordinate, and then the target blowout form was extracted by visual interpretation. At the same time, in order to compare the long-term expansion rate of blowouts, we also made a mosaic of aerial photographs taken in 1967 and compared them with these two high-resolution images taken in 2008, 2012 and 2015. But, due to the low resolution of the scanned B/W 1967 aerial photography and the very limited efficient control points available in the region, georeferencing and orthorectification processes with this kind of history image is very difficult established in prior studies. So, blowouts with an area smaller than 1000 m^2 are poorly visible on the photographs and could not be detected for comparison in similarity to previous researchers' experience (Jungerius and Meulen, Catena, 1989; Dech et al., Catena, 2005). Thus, only the medium sized blowouts (1000 m^2 < area < 10,000 m^2) and mega-blowouts (area > 10,000 m^2) margins can be identified and marked manually on screen with 1: 1000 enlargements of the airborne photos in ArcGIS software (version 10.0). The margins of the bare sand depositional lobes were clearly distinguishable from the surrounding and downwind grassland, and their positions were also measured. Only area, length and width of the three monitored target mega-

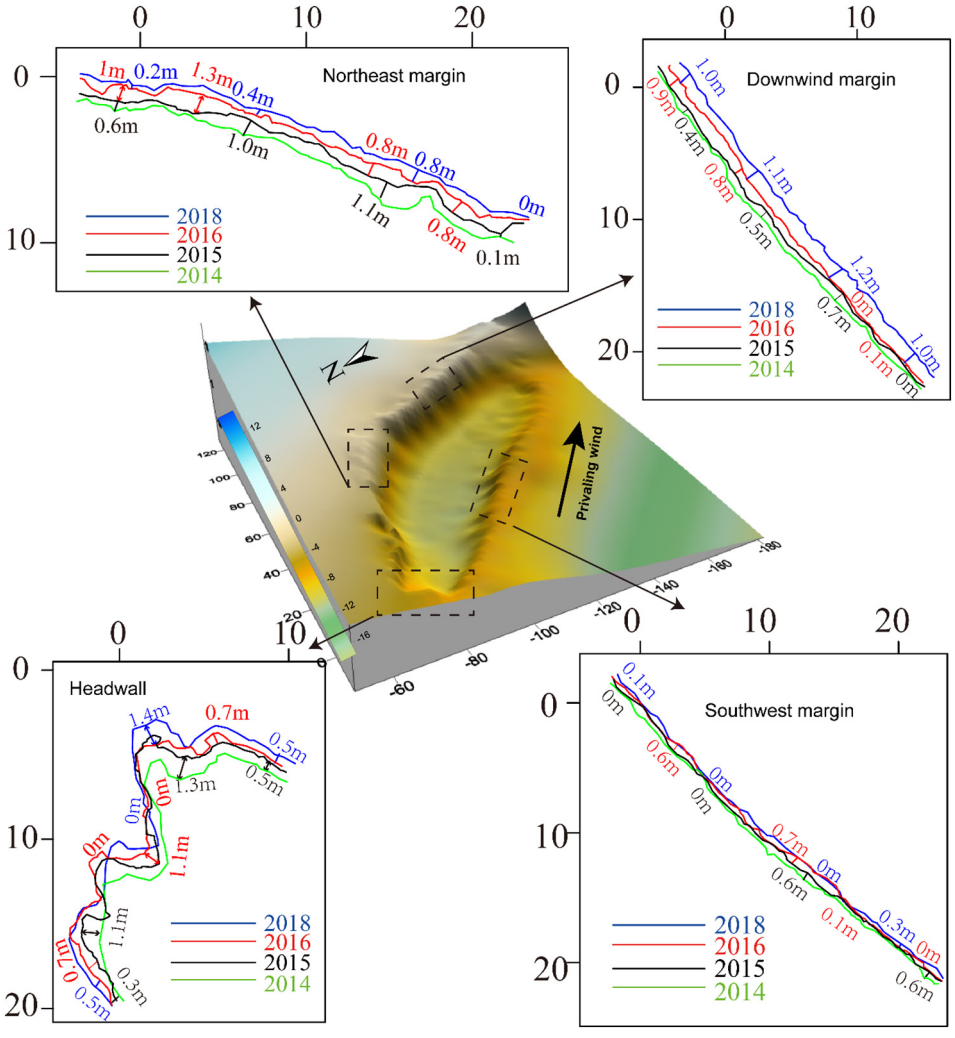

Fig. 6. The morphological margin expansion of monitored blowout B1.

blowouts (B1, B2 and B3 in Fig. 9, detailed data as shown in Table 2) were measured.

To assess the uncertainty of the scanned historical aerial photography, we have measured an onscreen distance between two target points (intersection of the road) on the aerial photos in ArcGIS software and made a comparison with the actual ground distance which we measured using RTK-GPS in field. The horizontal distance accuracy calculated through these distance ratios (onscreen/field) is 0.842 in this research. For the satellite images, orthorectification was performed ahead using the 7 m resolution DEM to eliminate the deformation. Then, registration and accuracy assessment were performed using the actual coordinates of the 11 ground control points (building corners, road intersections and farm fence intersections) which we have selected as far as possible as we can in the field to measure its precise coordinate using RTK-GPS, and access its accuracy. Table 1 and the online supplemental Fig. S1 shows the details of the control point distribution and their errors during registration.

3. Results

3.1. Blowout margin expansion rate from in-situ monitoring

During the periods of monitoring, the expansion rate varied between different sized blowouts and different parts of each blowout (Figs. 6–8). The headwall (upwind cliff edge, detailed definition see Fig. 5A,C) and the northeast sidewall of the blowouts appear to be the areas with the largest changes (Fig. 6), expanding on average 1.2 m a^{-1} (B1), 3.3 m a^{-1} (B2) and 0.4 m a^{-1} (B3). The fastest expansion rate is >6 m a^{-1} for B2. On the contrary, the topography of the downwind portion of the blowouts is relatively stable during the monitoring periods (Fig. 6). The average annual expansion rate of the northeast sidewall of the three blowouts is 1 m a^{-1}, 0.7 m a^{-1} and 0.3 m a^{-1}, respectively, with a maximum annual expansion rate in B1 and B2 of nearly 2 m a^{-1} (Fig. 7). The southwest side morphological changes of B1 shows a slightly faster rate than B2 and B3, with an annual average

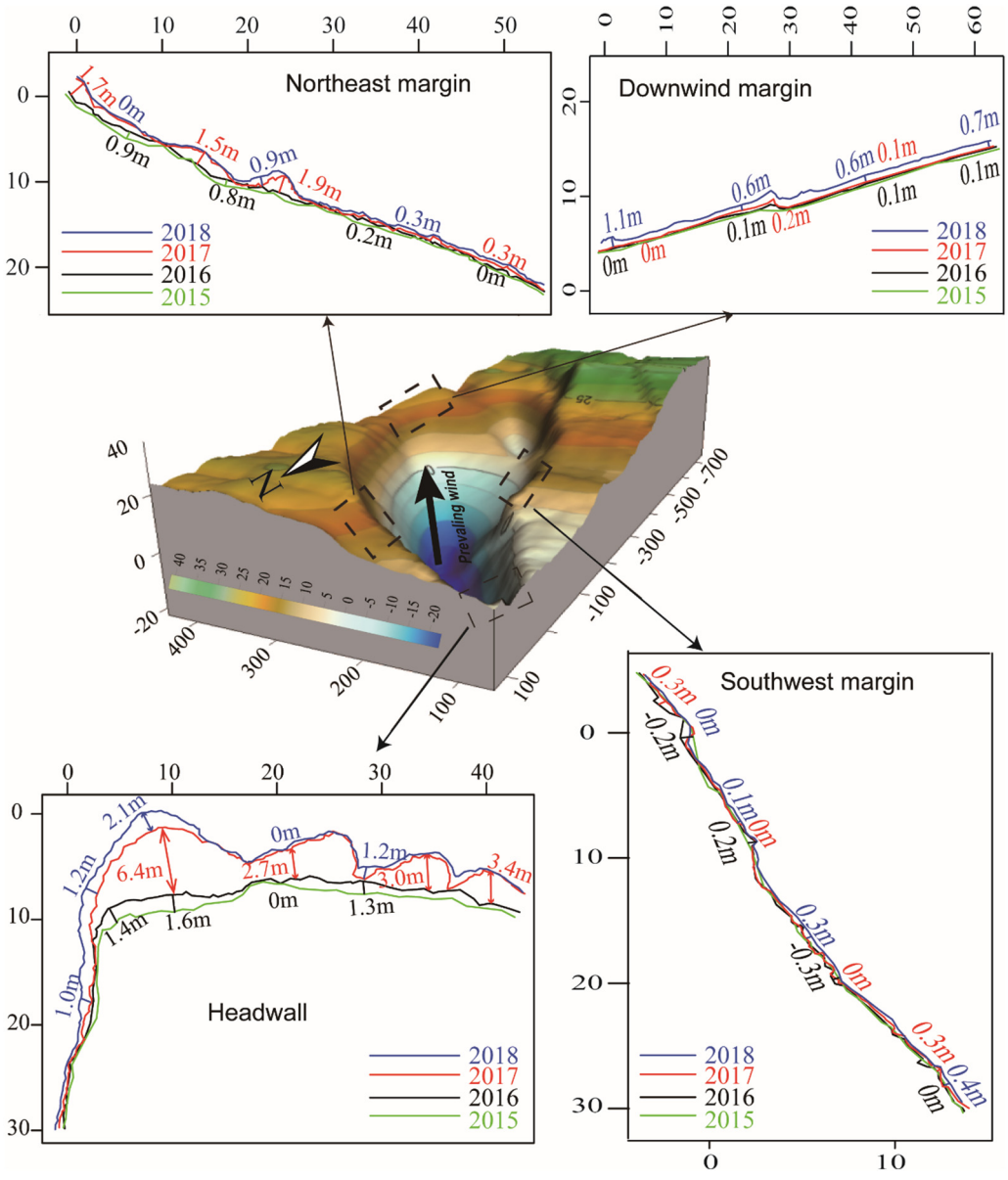

Fig. 7. The morphological expansion of monitored blowout B2.

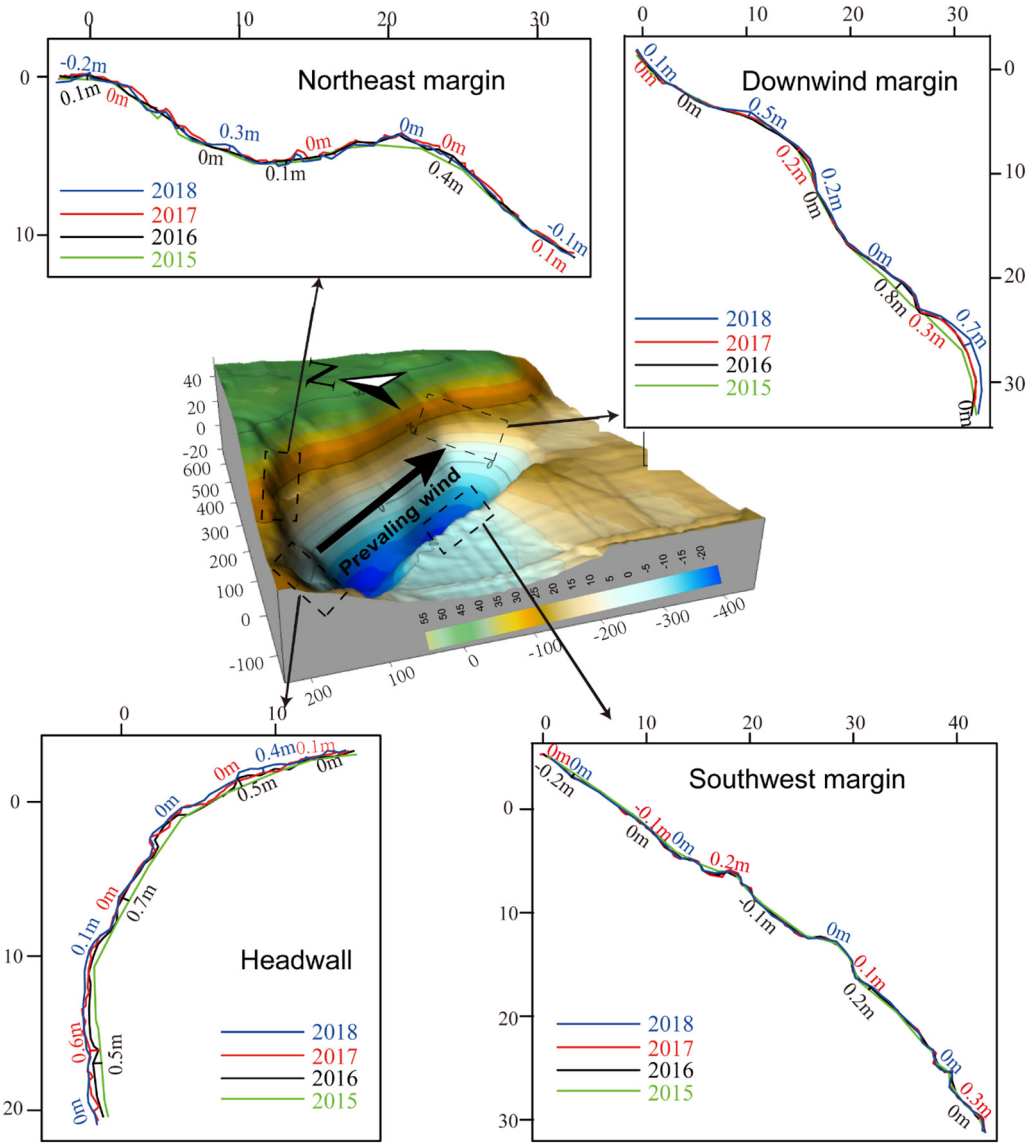

Fig. 8. The morphological expansion of monitored mega-blowout B3.

rate of about 0.5 m a^{-1}. The southwest sidewalls of the B2 and B3 blowouts were almost stable, showing a little expansion in some steep cliff portions with an annual lateral expansion rate of around 0.1 to 0.3 m, respectively (Fig. 8).

3.2. Long-term topographic change from remote-sensing data

Table 1 shows the longer historical expansion rates of the three monitored mega-blowouts of 41 years of evolution (1967 to 2008). It is clearly seen that the three monitored blowouts in Gonghe basin have experienced longitudinal rather than lateral expansion. The area of B1 expanded by nearly 24 times, much more rapidly than B2 and B3. B2 increased by 215 m in length and 17 m in width, with an annual expansion rate of 5.4 m a^{-1} and 0.43 m a^{-1}, respectively. The downwind depositional lobes of the blowouts also increased with the expansion of the deflation area (Fig. 9). The depositional lobe area of B1 grew most compared to B2 and B3, with an annual growth of over 2700 m^2 a^{-1}.

The marginal expansion of these three blowouts was still ongoing between 2008 and 2015, but the expansion rate had somewhat changed (Fig. 9). The area of B1 increased by 416 m^2, with an average annual change of 59.4 m^2 a^{-1}. The width of B1 increased by 6 m, but the length had changed little. The area of B2 increased by 6141 m^2, with an average annual growth of 877.30 m^2 a^{-1}. The length of B2 and B3 increased by 12 m and the width showed no significant change (an increase of only 2 m for B2) within 7 years. B3's rate of expansion, supported by field observations, had slowed suggesting perhaps that blowout B3 has reached a more mature stage.

3.3. Blowout evolution processes

With the aid of satellite images and aerial photographs, we found that the development of the blowouts is not an independent process and frequent interactions may occur with adjacent blowouts and sand patches, as also observed by Abhar et al. (2015) for example. Side-by-side and tandem merging are the two dynamic development processes that occur during the mega-blowout evolution. Side-by-side merging usually occurs between two close neighbor blowouts. In 2008, the minimum distance between two blowouts, S1 and S2, was about 7 m, but they were closer in 2012 (3 m apart) and completely connected in 2015 (Fig. 10A). Tandem merging refers to the situation where two aligned blowouts connected to each other along with the prevailing wind direction during their development. As shown in Fig. 10, there is still an erosion remnant edge of about 10 m between the two blowouts T1 and T2 in 2008 and 2012, but these blowouts have been connected

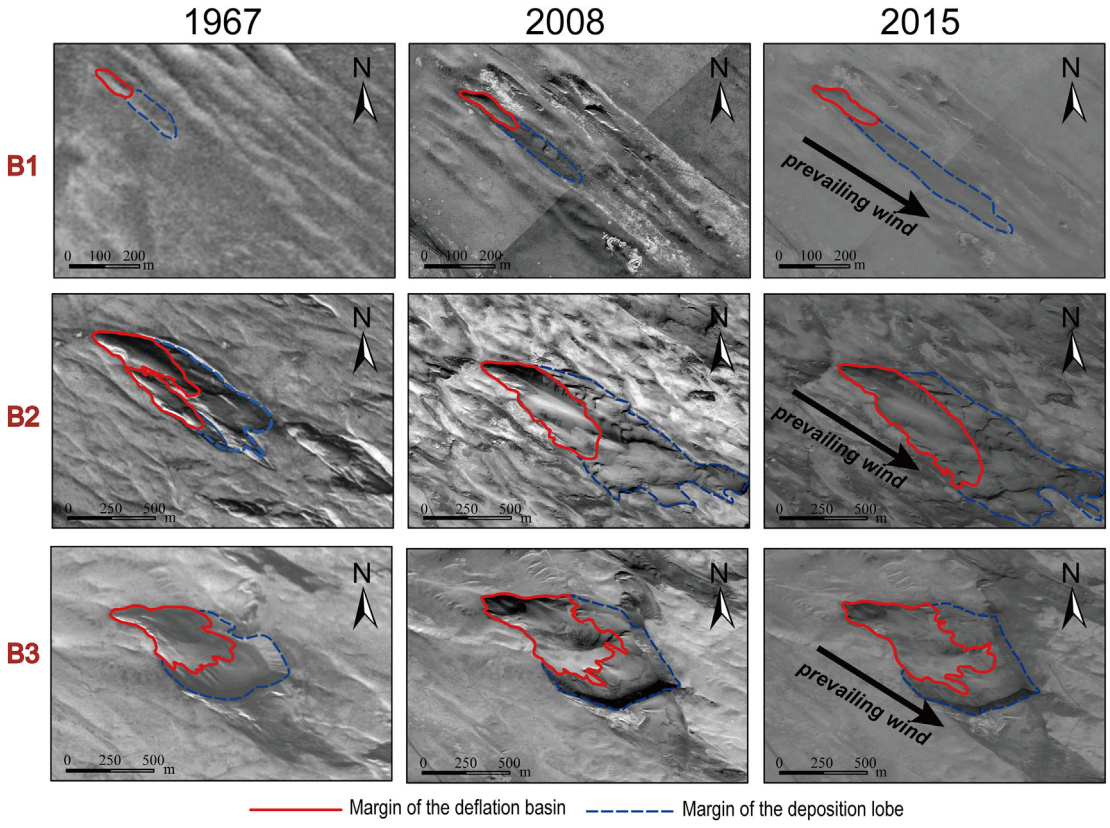

Fig. 9. Historical expansion of monitored mega-blowouts from 1967 to 2015. (Aerial image and satellite image comparisons).

and merged into a single larger blowout T12 in 2015 (Fig. 10B). At the same time, the distance between T2 and T3 is also becoming less, and contracted >1.5 m from 2008 to 2015. Data collected during the recent field survey on January 2018, shows that the two blowouts T2 and T3 have now completely merged together.

Sand patch merging is an important process during the early stage development of blowouts, and the merging direction is always uncertain. After the merging is completed, it becomes a typical blowout (Fig. 10C). Meanwhile, the margin of the blowouts will gradually become smooth with the merging and evolution process, reflecting the adaptation of the form to the local airflow.

4. Discussion

4.1. Differences in blowout evolution between alpine regions and coastal regions

The cold alpine desert region in the north-eastern QTP is a unique aeolian environment due to its low temperature and low air pressure. Vegetation growth in this region is very slow, whilst soils are affected by freeze-thaw processes and prolonged periods of snow cover. The environmental conditions are similar to those observed in arctic and subarctic coastal environments (Ruz and Hesp, 2014). This harsh natural environment fundamentally affects the formation, stabilization, and reactivation of sand dunes. It is therefore interesting to compare blowouts developed in the QTP with blowouts in other environments.

Due to the difference in the length of the slump slopes (Fig. S2) and the heights of the cliffs/depths of the blowouts (Fig. 5C, D, E), the energy balance within the mega-blowouts in the QTP is often influenced by local topography and slope orientation, which affects the incidence angle of solar radiation and the vegetation growth that depends on it. Furthermore, blowouts in coastal regions and low altitude desert regions may be transformed to barchan and parabolic dunes (Hugenholtz and Wolfe, 2006; Hesp and Walker, 2013). However, the downwind depositional lobes of both the mega-trough blowouts and the smaller sized blowouts are still experiencing ongoing extension, free of stabilization by shrubs and grasses. The lack of development of the QTP blowouts into parabolic dunes is most likely due to the presence of short grass only in the region and, therefore, trailing ridges which characterise parabolic dunes do not develop. Also, compared to the coastal blowouts, and probably some semi-arid to desert region blowouts, the massive thickness of the paleo-aeolian deposits on which the mega-blowouts are initiated and develop lies 500 m above the water level of the Yellow River and the water table is very deep (Xu et al., 1984; Dong et al., 1993). Thus, unlike coastal environments where deflation can relatively quickly reach a water table or other hard substrate (Hesp, 2002), there is no seasonal water table limiting continuous erosion in the deflation basin once the initial stage blowout is formed (Luo et al., 2018).

4.2. What causes variations in blowout expansion rates?

First, we consider the differences in the four-years monitored expansion rates across the three different QTP mega-blowouts. B2 shows the most active expansion, and B3 the least. Margin expansions were consistent with headwalls showing rapid up-wind expansion, northeast side wall deformation and expansion the next most eroding sites, and the southwest edges the least. Headwall erosion is not uncommon in some blowouts (e.g. Adamson et al., 1988; Jungerius et al., 1981; Carter et al., 1990; Pluis, 1992). There are two main reasons for the uneven growth of both sides of the QTP blowouts. Firstly, due to more direct sunlight exposure on the northeast side of the blowouts, the moisture content is low, suppressing vegetation growth in summer and annual temperature range is greater, enhancing freeze-thaw cycles. The additional heating and drying of the NE walls means that slumping and avalanching is greater on that side compared to the opposite side, and therefore, retreat is greater on the NE side (cf. Hugenholtz and Wolfe, 2006).

Secondly, the growth modes of different blowouts are dissimilar because they are in different evolutionary stages. The average annual area

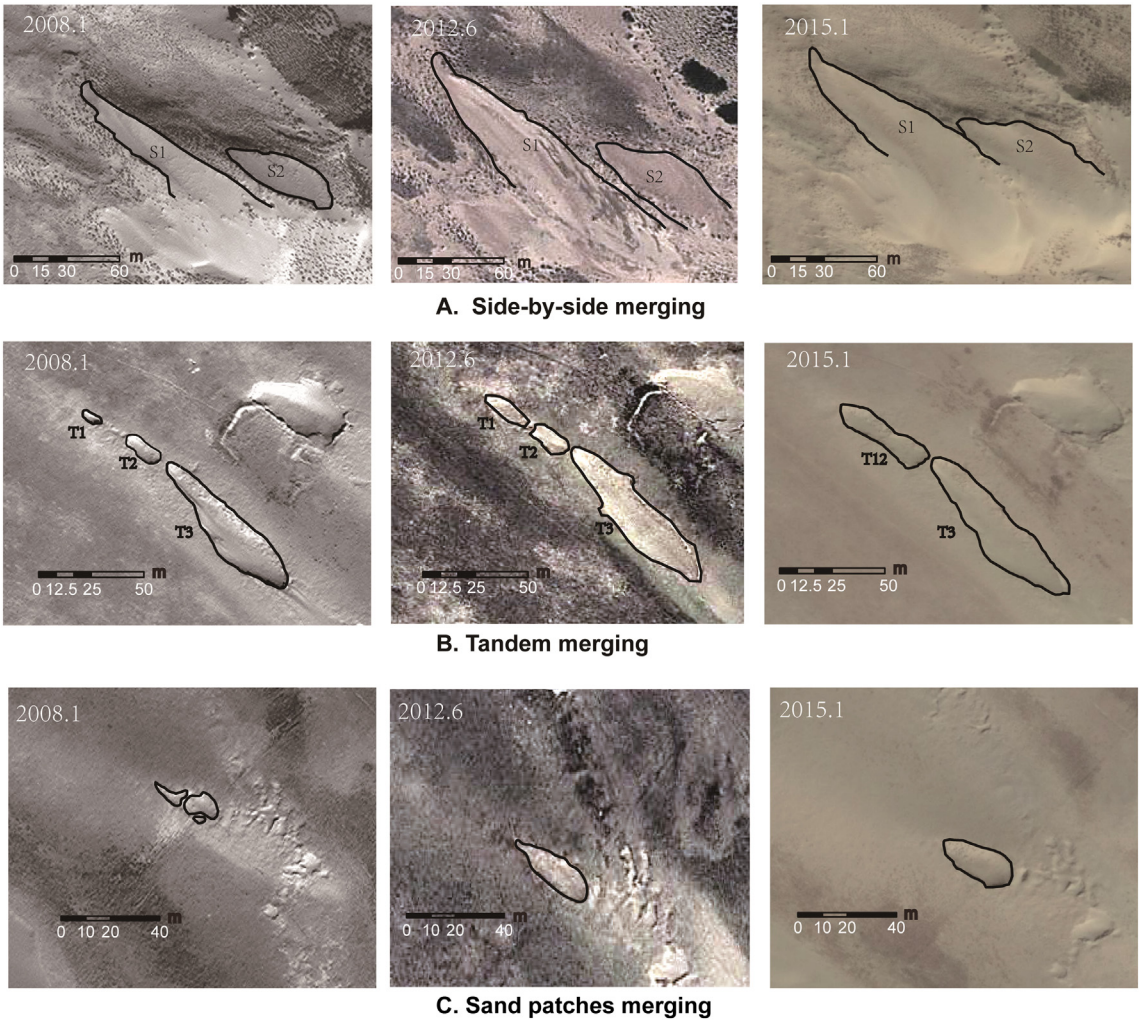

Fig. 10. Blowouts dynamical development and evolution processes reflected by historical images analysis.

growth of B2 in 2008–2015 was significantly faster than that of 1967–2008, the growth rate of B3 appears to have been slowing, and that of B1 is fairly consistent in these two different periods. Ascertaining the exact factors of mega-blowout expansion may be further complicated by the changing response of mega-blowouts as they evolve. According to the topographic expansion modes of the three different sized blowouts, it seemed that there exists a critical size/area threshold in their development; B3 is the first deflation basin to reach this critical size, and its form no longer continues to expand. However, before reaching the critical size, the form of B3 in 1967–2008 experienced a rapid growth stage, one which the present B2 appears to be experiencing currently.

4.3. Initiation and controls of the mega-blowout evolution in QTP

Hesp (2002) stated that factors inducing blowout initiation included water erosion, airflow acceleration due to terrain, climate change, disturbance to vegetation successional trends, fire, wave and wind erosion, and human and animal impacts. Our field monitoring and surveys during the four-year survey period indicate that the initiation processes and the controlling factors that have governed the development and evolution of blowouts in the QTP are more complex than in coastal systems, though wind is considered as the primary force.

4.3.1. Sedimentary environments

The composition and structure of the base sediments can determine their vulnerability to wind erosion and hence the mega-blowout formflow feedback behaviour. Aeolian archives in the northern plateau have much more diverse geographical backgrounds, with elevations ranging from 2500 m to >4000 m. The thickness and extent of aeolian deposits in this region are complex due to there being multiple sources of aeolian sediments (Dong et al., 1993). Mega-blowouts in Gonghe basin are mainly formed in the palaeodunes on the terrace of the Yellow River. Field data shows these palaeodunes to have a thick vegetated top surface soil layer and a loose sandy substrate (Fig. 5C, D). Once the top surface layer is disrupted there is ample loose sandy sediment available for mega-blowout formation and development. Furthermore, as we observed in our field survey, once blowouts are initiated, the partial induration of the clayey sediments leads to large block collapse from the top clay layer and this accelerates lateral expansion. Scarce vegetation cover, low moisture contents and deep sands in the Gonghe basin provide the material basis to form such massive deflational landforms and maintain their continued growth for timescales of at least decades.

4.3.2. Surface disturbance and wind regime

The typical soil profile in the Gonghe basin is composed of a thin, vegetation-bound top layer and poorly cemented sandy sub-layer which has high wind erodibility (Fig. 5D). The underlying sediments are exposed to the wind wherever the vegetation cover is removed, which provide dynamic conditions for wind erosion. Therefore, any factors such as drought, overgrazing, modern traffic activity (vehicles, four-wheel drive), and freezing-thawing can disturb the fragile

vegetated top soil surface, and enhance the blowouts initiation and wind-driven land degradation processes (Fig. 11).

Once surface erosion by strong winds occurs, aeolian processes act to remove, undermine and bury vegetation and create a sand patch. Continued deflation creates concave blowouts which then extend downwind and laterally due to side wall aeolian abrasion and by collapse, deflation basin deepening and elongation, and associated development and extension of the depositional lobe.

4.3.3. Water erosion

Even though precipitation in the blowouts in north-eastern QTP, especially in the Gonghe basin, is low in summer, in some cases, heavy precipitation can still generate short-term overland flow on the marginal slopes of the blowouts causing gully erosion and collapse. Fig. 12 shows the gully erosion on the side wall and the bottom of the deflation basin in B3. It clearly reflects that the water erosion not only enhanced the cliff collapse to form a steeper and more concave sidewall, but also provided more loose sediments for wind erosion and promoted air flow separation and generated more turbulence and vorticity, thus speeding the form-flow feedback and enhancing the expansion rate (cf. Hugenholtz and Wolfe, 2009). Accordingly, we believe that water erosion plays a secondary shaping role in the mega-blowouts evolution, as has also been observed in the development of blowouts in the Netherlands (e.g. Jungerius et al., 1981; Pluis, 1992).

4.3.4. Freeze-thaw cycle

Our consecutive observations indicate that freeze-thaw cycles play a key role on the process of formation and evolution of blowouts in the high-altitude alpine regions in the north-eastern QTP. There are two basic ways for the freeze-thaw cycle processes to influence blowout formation and their evolutionary processes: freeze-thaw cracking and freeze-thaw collapse. In the neighbouring Zoige Basin, where periglacial processes are more active, formation of blowouts by freeze-thaw processes has been observed. No observations have been made of this occurring in Gonghe at present, but paleoenvironmental data suggest the region was colder 200–500 years ago (Yang et al., 2014), and patchy permafrost may exist in north-eastern QTP (Ran et al., 2018). So, freeze-thaw may also have triggered some blowout formation in Gonghe basin (Yang et al., 2014; Luo et al., 2018). Active, freeze-thaw processes crack the grassland surface forming polygons (Fig. 13A). Once formed, the airflow can be accelerated along the gaps within these polygons, inducing airflow funnelling and turbulence which enhances the entrainment of fine particles in the top clay layer, and hence causes crack enlargement, surface vegetation mortality and erodibility, accelerating crack formation and thaw patch size (Fig. 13C). Thereby, the surface albedos are changed with more solar energy being absorbed by the bare sandy patches, which then increase the freeze-thaw processes. Through time, the cracks enlarge further and merge together (Fig. 13D, E). Once sufficient bare sand is exposed, the strong wind deflates the loose sand and triggers the blowout formation (Fig. 13F).

Freeze-thaw processes also promote side wall collapse in the mega-blowouts in spring. According to our field observations, in the cold season, the freezing and thawing activity increases the fracture density of the soil. Melting in the spring then gives rise to massive failure with sandy/clayey blocks collapsing under the action of gravity. Fig. 14 shows the cliff wall collapse observed during the terrain monitoring in Gonghe basin in March, 2016. The biggest collapse block is 2 m long in its long axis, and 1 m long in the short axis, which means that the edge expansion rate caused by this collapse is at least 1 to 2 m. This kind of huge block collapse causes sudden and significant morphological change. During the monitoring periods, we also found that the relative height and slope of the headwall and sidewalls affects the efficacy of block collapse. The height of the headwall of the B2 blowout is up to 3 m and the expansion rate is the largest. In contrast, the height of the headwall of B1 and B3 is less than 1 m, the gravity erosion is weaker, and their expansion rate is lower.

4.3.5. Anthropogenic influences and climate

Even though the mega-blowouts in Gonghe basin may have been initiated hundreds of years ago, and the impacts of human activities at

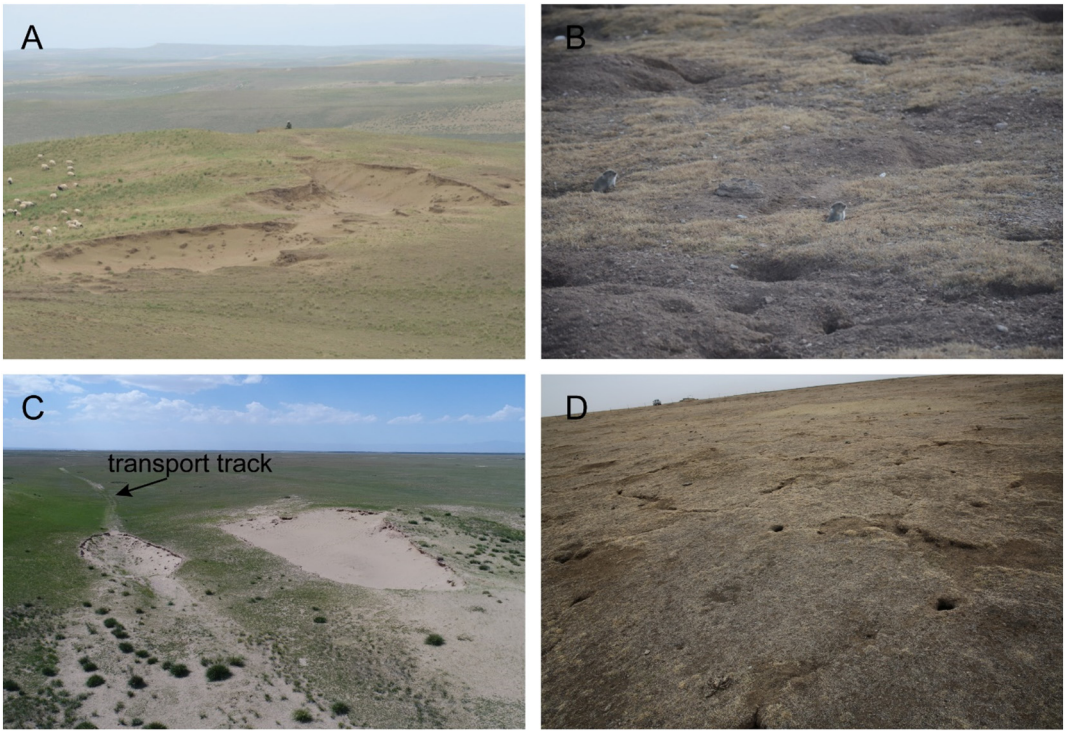

Fig. 11. Factors triggering the surface disturbance and blowout formation. A) Over-grazing leading to two blowouts merging together; B. burrows of Pika as a serious disturbance of the grassland in QTP; C. vehicle tracks destroy the top surface vegetation layer and induce wind erosion along the track; D, freeze-thaw cycle cracked polygons on the top of grassland also providing conditions for wind erosion to occur in these gaps to form sand patches.

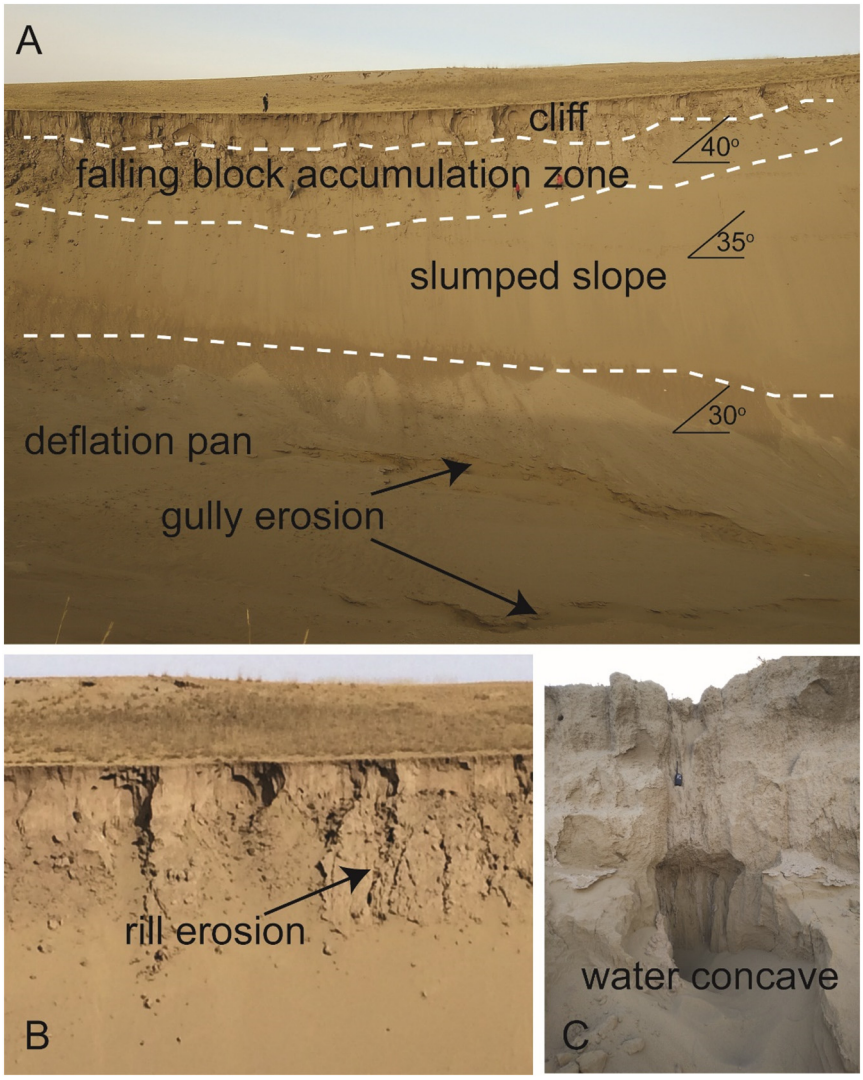

Fig. 12. Gully erosion of the blowouts side wall and plain by a storm rain event in the rainy season. A). deflation plain gully erosion; B. side wall rill erosion; C. side wall concave water erosion.

that time were less than today, the newest smaller sized blowouts formed recently in the region are likely related to current and ongoing anthropogenic impacts such as habitation, over-grazing, farming, mining and modern transportation. According to previous research, both climate changes and anthropogenic disturbances have caused wind-driven land degradation in the region (Li et al., 2010; Dong et al., 2017). Vegetation growth and cover has declined in recent decades due to a significant increase in grazing of the grasslands and more intensive human activities (Fig. 15). In addition, humans and livestock can also enhance the rate of sidewall collapse process by trampling and destabilizing the margins around the blowouts. Modern transport, especially four-wheel drive activities can destroy the vegetated surface, leaving the loose sandy substrate free for wind erosion. Furthermore, the temperature and drought level in this region are increasing (Dong et al., 2017) (Fig. 3A) which may be contributing to mega-blowout expansion by suppressing vegetation cover and growth.

5. Conclusion

1) Mega-blowouts have developed in the Gonghe basin on the Qinghai-Tibet Plateau due to an almost unlimited depth of sand, very low water table, and short grassland, thereby significantly limiting their evolution into parabolic dunes.
2) Four years in-situ topographic monitoring results show the three monitored mega-blowouts displayed short and long-term expansion rates which varied both between different sized blowouts and within different parts of each blowout. Headwall upwind expansion appears greatest followed by the northeast side wall. Longitudinal expansion is greater than the lateral expansion, and the growth of the depositional lobes is faster than the growth of the deflation basins.
3) Merging of adjacent sand patches and blowouts are the key process for mega-blowout development and extension.
4) Sediment characteristics, water erosion, and freeze-thaw processes all play a part in mega-blowout initiation and expansion. However, the relative roles that these factors play may differ according to a blowout's different evolutionary stages.
5) Emergence of new sand patches and small blowouts around the mega-blowouts in the research area suggests that land degradation is still an ongoing process. Future in-situ measurements and simulation work needs to be conducted in order to understand the feedback mechanisms between the blowout morphodynamics, climate change and anthropogenic influences or impacts.

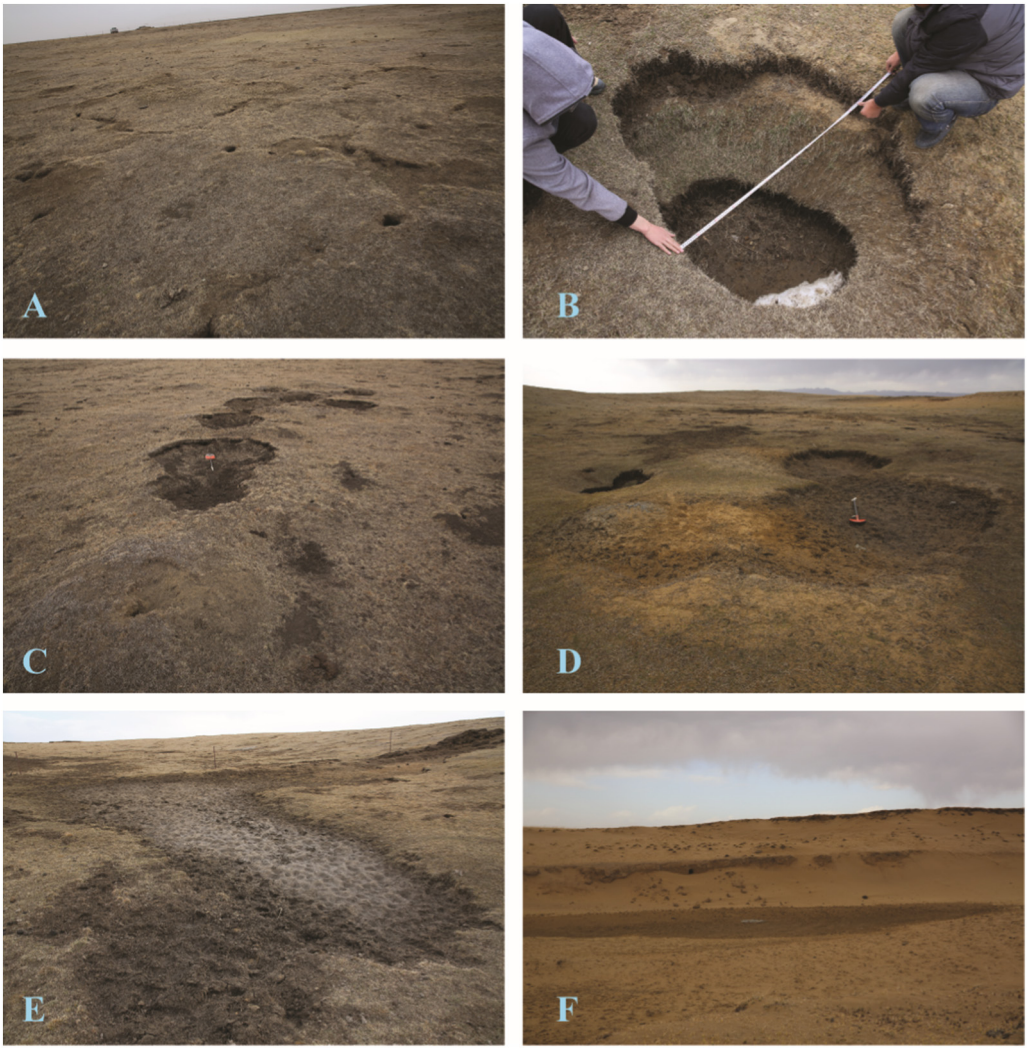

Fig. 13. Freeze-thaw cycle induced formation and evolution of blowouts in high altitude alpine regions in the Zogil basin. A. Freeze-thaw polygon B. Freeze-thaw cavity C. Freeze-thaw patches D. Patches merge, sandy layer exposed E. Meadow disappeared and sand sheet spreading F. Blowout formation and expansion.

Fig. 14. Freeze-thaw induced fracture and side wall collapse during the Spring season in Gonghe basin blowouts.

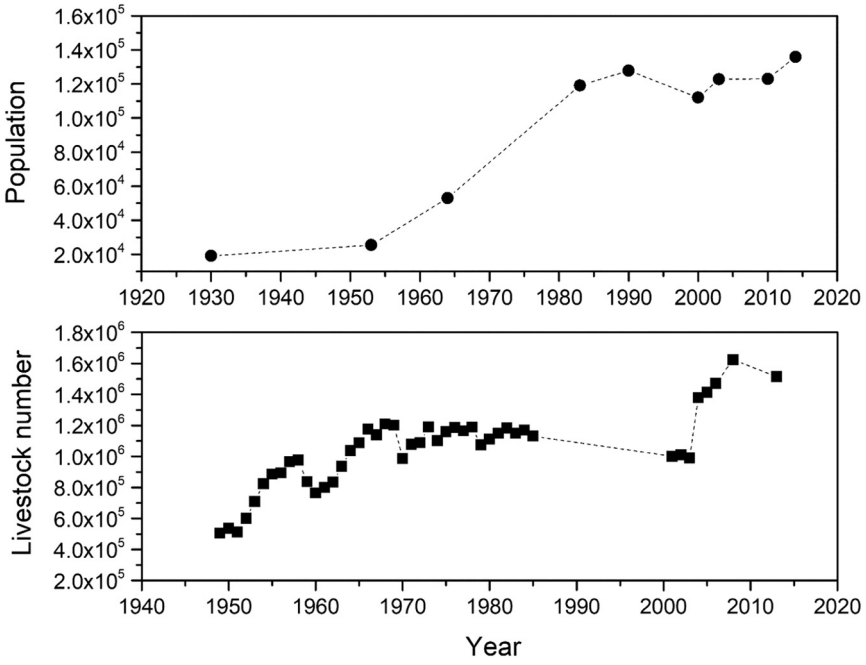

Fig. 15. Grazing capacity and population growth in the past decades in Gonghe.

Acknowledgments

The authors wish to express their thanks for the valuable field assistance provided by many individuals over the course of this study and, in particular to Zhendong Ma, Shuzhi Ji, Mingliang Tan, Zhengqiang Qi. Permission to conduct the research and additional logistical support was provided by Huoxian Yang and his family. Many thanks to Felix Ng and Robert Bryant for their valuable suggestions and discussions. The constructive comments from the editor Andrew Plater and two anonymous reviewers are appreciated. This research was supported by National Natural Science Foundation of China (41371026; 41771015) and Key Project from the Ministry of Science and Technology of the People's Republic of China (2013CB956003). Wanyin Luo acknowledges the wonderful support from the China Scholarship Council and the University of Sheffield for hosting him as an academic visitor. Patrick Hesp sincerely thanks the China Academy of Sciences for a PIFI scholarship.

Appendix A. Supplementary data

Supplementary data to this article can be found online at https://doi.org/10.1016/j.geomorph.2018.12.033.

References

Abhar, K.C., Walker, I.J., Hesp, P.A., Gares, P.A., 2015. Spatial-temporal evolution of Aeolian blowout dunes at Cape Cod. Geomorphology 236, 148–162.
Adamson, D.A., Selkirk, P.M., Colhoun, E.A., 1988. Landforms of Aeolian, tectonic and marine origin in the Bauer Bay-Sandy Bar region of subantarctic Macquarie Island. Pap. Proc. R. Soc. Tasmania 122, 65–82.
Barchyn, T.E., Hugenholtz, C.H., 2013. Dune field reactivation from blowouts: Sevier Desert, UT, USA. Aeolian Res. 11, 75–84.
Carter, R.W.G., Hesp, P.A., Nordstrom, K.F., Nordstrom, K.F., Psuty, N.P., Carter, R.W.G., 1990. Erosional landforms in coastal dunes. Coastal Dunes. J. Wiley and Sons, pp. 217–250.
Cooper, W.S., 1958. Coastal sand dunes of Oregon and Washington. The Geological Society of America Memoir 72. Waverly Press, Baltimor.
Dech, J.P., Maun, M.A., Pazner, M.I., 2005. Blowout dynamics on Lake Huron sand dunes: analysis of digital multispectral data from colour air photos. Catena 60, 165–180.
Dong, G.R., Gao, S.Y., Jin, J., 1993. Aeolian Desertification and its Control in Gonghe Basin of Qinghai Province. (in Chinese with English summary). Science Press, Beijing.
Dong, Z.B., Hu, G.Y., Qian, G.Q., Lu, J.F., Zhang, Z.C., Luo, W.Y., Lyu, P., 2017. High-altitude Aeolian research on the Tibetan Plateau. Rev. Geophys. https://doi.org/10.1002/2017RG000585.
Fraser, G.S., Bennet, S.W., Olyphant, G.A., Bauch, N.J., Ferguson, V., Gellasch, C.A., Millard, C.L., Mueller, B., O'Malley, P.J., Way, J.N., Woodfield, M.C., 1998. Windflow circulation patterns in a coastal dune blowout, south coast of Lake Michigan. J. Coast. Res. 14, 451–460.
Fryberger, S.G., Dean, G., 1979. Dune forms and wind regime. In: McKee, E.D. (Ed.), A Study of Global Sand Seas. University Press of the Pacific, Honolulu, pp. 137–170.
Gares, P.A., Nordstrom, K.F., 1995. A cyclic model of foredune blowout evolution for a leeward coast: Island Beach, NJ. Ann. Assoc. Am. Geogr. 85, 1–20.
Hesp, P., 2002. Foredunes and blowouts: initiation, geomorphology and dynamics. Geomorphology 48, 245–268.
Hesp, P.A., Hyde, R., 1996. Flow dynamics and geomorphology of a trough blowout. Sedimentology 43, 505–525.
Hesp, P.A., Pringle, A., 2001. Wind flow and topographic steering within a trough blowout. J. Coast. Res. SI 34, 597–601.
Hesp, P.A., Walker, I.J., 2012. Three-dimensional aeolian dynamics within a bowl blowout during offshore winds: Greenwich dunes, Prince Edward Island, Canada. Aeolian Res. 3, 389–399.
Hesp, P.A., Walker, I.J., 2013. Coastal dunes. In: Shroder, J., Lancaster, N., Sherman, D.J., Baas, A.C.W. (Eds.), Treatise on Geomorphology. Aeolian Geomorphology vol. 11. Academic Press, San Diego, CA, pp. 328–355.
Hesp, P.A., Smyth, T.A.G., Walk, I.J., Gares, P.A., Wasklewisz, T., 2016. Flow within a trough blowout at Cape Cod. J. Coast. Res. SI 75, 288–292.
Hesp, P.A., Hilton, M., Konlecher, T., 2017. Flow and sediment transport dynamics in a slot and cauldron blowout and over a foredune, Mason Bay, Stewart Island (Rakiura), NZ. Geomorphology 295, 598–610.
Hugenholtz, C.H., Wolfe, S.A., 2006. Morphodynamics and climate controls of two Aeolian blowouts on the northern Great Plains, Canada. Earth Surf. Process. Landf. 31, 1540–1557.
Hugenholtz, C.H., Wolfe, S.A., 2009. Form–flow interactions of an Aeolian saucer blowout. Earth Surf. Process. Landf. 34, 919–928.
Jungerius, P.D., Meulen, F.V.D., 1989. The development of dune blowouts, as measured with erosion pins and sequential air photos. Catena 16, 369–376.
Jungerius, P.D., Verheggen, A.J., Wiggers, A.J., 1981. The development of blowouts in 'De Blink', a coastal dune area near Noordwijkerhout, The Netherlands. Earth Surf. Process. Landf. 6, 375–396.
Jungerius, P.D., Witter, J.V., van Boxel, J.H., 1991. The effects of changing wind regimes on the development of blowouts in the coastal dunes of The Netherlands. Landsc. Ecol. 6, 41–48.
Li, S., et al., 2010. Wind-Driven Land Degradation and its Control in Xizang Tibet. (in Chinese with English summary). Science Press, Beijing.
Liu, B., Jin, H.L., Sun, L.Y., Sun, Z., Su, Z.Z., Zhang, C.X., 2013. Holocene climatic change revealed by Aeolian deposits from the Gonghe Basin, northeastern Qinghai-Tibetan Plateau. Quat. Int. 296, 231–240.
Luo, W.Y., Wang, Z.Y., Lu, J.F., Yang, L.H., Qian, G.Q., Dong, Z.B., Bateman, M.D., 2018. Mega-blowouts in Qinghai-Tibet Plateau: morphology, distribution and initiation. Earth Surf. Process. Landf. https://doi.org/10.1002/esp.45r07.
Nield, J.M., Baas, A.C.W., 2008. Investigating parabolic and Nebkha dune formation using a cellular automaton modelling approach. Earth Surf. Process. Landf. 33, 724–740.
Pluis, J.L.A., 1992. Relationships between deflation and near surface wind velocity in a coastal dune blowout. Earth Surf. Process. Landf. 17, 663–673.
Qiang, M.R., Jin, Y.X., Liu, X.X., Song, L., Li, H., Li, F.S., Chen, F.H., 2016. Late Pleistocene and Holocene Aeolian sedimentation in Gonghe Basin, northeastern Qinghai-Tibetan Plateau: variability, processes, and climatic implications. Quat. Sci. Rev. 132, 57–73.

Ran, Y.H., Li, X., Cheng, G.D., 2018. Climate warming over the past half century has led to thermal degradation of permafrost on the Qinghai–Tibet Plateau. The Cryosphere 12, 595–608.
Ruz, M.H., Hesp, P.A., 2014. Geomorphology of high-latitude coastal dunes: a review. Geol. Soc. Lond. Spec. Publ. 388, 199–212.
Smyth, T.A.G., Jackson, D.W.T., Cooper, J.A.G., 2012. High resolution measured and modelled three-dimensional airflow over a coastal bowl blowout. Geomorphology 177–178, 62–73.
Villanueva, R.G., Costas, S., Duarte, H., Perez-Arlucea, M., Alejo, I., 2011. Blowout evolution in a coastal dune: using GPR, aerial imagery and core records. J. Coast. Res. 64, 278–282.
Xu, S.Y., Xu, D.F., Shi, S.R., 1982. Aeolian sand deposits in the Gonghe Basin, Qinghai province. (in Chinese with English abstract). J. Desert Res. 2, 1–8.
Xu, S.Y., Xu, D.F., Shi, S.R., 1984. A discussion on the development of landforms and evolution of environments in the Gonghe Basin. (in Chinese with English abstract). J. Lanzhou Univ. 20, 146–157.
Yan, N., Baas, A.C., 2015. Parabolic dunes and their transformations under environmental and climatic changes: towards a conceptual framework for understanding and prediction. Glob. Planet. Chang. 124, 123–148.
Yang, B., Qin, C., Wang, J.L., He, M.H., Melvin, T.M., Osborn, T.J., Briffa, K.R., 2014. A 3,500-year tree-ring record of annual precipitation on the northeastern Tibetan Plateau. PNAS 111, 2903–2908.
Zhang, J., 1991. County Chronicles of Gonghe. (in Chinese). Qinghai Renming Press, Xining, pp. 67–87.
Zhang, D.P., Wang, X.K., Hasi, E.D., Sun, H.W., Zhao, J.M., Liu, X., Feng, Z.W., 2006. Hulun Buir sandy grassland blowouts: geomorphology, classification and significances. (in Chinese with English abstract). J. Desert Res. 26, 894–902.